Reversible plastic events in amorphous materials

Micah Lundberg,[1] Kapilanjan Krishan,[1] Ning Xu,[2,3] Corey S. O'Hern,[4,5] and Michael Dennin[1]
[1]*Department of Physics and Astronomy, University of California at Irvine, Irvine, California 92697-4575, USA*
[2]*Department of Physics and Astronomy, University of Pennsylvania, Philadelphia, Pennsylvania 19104-6396, USA*
[3]*James Franck Institute, The University of Chicago, Chicago, Illinois 60637, USA*
[4]*Department of Mechanical Engineering, Yale University, New Haven, Connecticut 06520-8286, USA*
[5]*Department of Physics, Yale University, New Haven, Connecticut 06520-8120, USA*
(Received 13 September 2007; revised manuscript received 8 February 2008; published 15 April 2008)

For crystalline materials, the microscopic origin of plasticity is well understood in terms of the dynamics of topological defects. For amorphous materials, the underlying structural disorder prevents such a description. Therefore identifying and characterizing the microscopic plastic events in amorphous materials remains an important challenge. We show direct evidence for the coexistence of reversible and irreversible plastic events (T1 events) at the microscopic scale in both experiments and simulations of two-dimensional foam. In the simulations, we also demonstrate a link between the reversibility of T1 events and pathways in the potential energy landscape of the system.

DOI: 10.1103/PhysRevE.77.041505 PACS number(s): 83.50.−v, 05.70.Ln, 05.20.Gg, 83.80.Iz

A fundamental question in materials science is identifying the microscopic origin of plasticity. Why do materials display plastic rather than elastic response and can we predict when this will occur? An improved understanding of plastic deformation is important in a wide range of amorphous materials, such as metallic [1,2] and polymeric glasses [3], foams [4], granular materials [5], colloids [6,7], and emulsions [8]. In crystalline materials, plastic behavior is understood in terms of defect nucleation and dynamics [9,10]. For amorphous materials, a description in terms of topological defects is not possible due to the inherent structural disorder. Therefore identifying and characterizing local plastic events in amorphous materials is essential for a complete understanding of their structural and mechanical properties.

The macroscopic response of amorphous solids and complex fluids, such as foams, colloids, and granular matter, to applied stress and strain is very similar: elastic at small strains and plastic at larger strains. In the elastic regime, stress is proportional to applied strain, and deformations are reversible. Above the yield stress or strain, an elastic deformation and plastic flow occur. Many models of plasticity in amorphous materials have emphasized the importance of microscopic "plastic zones" containing at most tens of particles [2,11–16] in which neighbor switching and other rearrangements events of "particles" occur. The particles represent atoms or molecules in the case of solids, or bubbles or grains in the case of complex fluids. When the elastic regions surrounding the microscopic plastic zones fail, macroscopic plastic flow can develop.

We perform both experiments and simulations of two-dimensional amorphous foams undergoing oscillatory shear strain to investigate the dynamics of microscopic plastic zones. In both cases, we find a coexistence of reversible and irreversible plastic rearrangement events at the microscopic scale, even for strains significantly above the yield strain [17]. The simulations provide critical insight into the mechanisms of reversibility. In the simulations, measurements of the local potential energy allow us to assess the impact of the surrounding bubbles on the reversibility of plastic events in ways that are not possible in the experiments. We argue that above the yield stress or strain, whether or not a microscopic plastic zone is reversible is determined by the available pathways in the potential energy landscape that allow the system to move from one configuration to another, and not simply the energetic stability of the configuration.

The experiments used bubble rafts [18–21] consisting of gas bubbles floating on a water surface. Simulations employed the well-characterized bubble model for two-dimensional (2D) foams developed by Durian [22]. Experimental evidence supports the applicability of the bubble model to explain the flow behavior of bubble rafts, as well as three-dimensional foam [21,23,24]. Even though other plastic rearrangement events occur in bubble rafts and the bubble model, we will focus on reversible and irreversible plastic events (T1 events) since they play a central role in foam [20,21,25–31].

T1 events correspond to a neighbor switching event in which two neighboring bubbles lose contact, and two next-nearest neighbors become neighbors [4]. This corresponds to a transition between two distinct states of the system. For example, referring to Fig. 1, state A is when bubbles 1 and 2 are neighbors, and state B is when bubbles 3 and 4 are neighbors. For both the experiment and simulations, during one cycle the applied shear strain varies from 0 to A/L_y (at phase $\psi=\pi$) and back to a strain of 0 (at $\psi=2\pi$), where A is the amplitude of the shear displacement and L_y is the system size in the shear-gradient direction. If four bubbles experience a T1 event that switched the bubbles from state A to B during the first half-cycle of the drive, a reversible T1 event occurs if the same foursome of bubbles returns to state A in the second half-cycle of the drive. Otherwise, the T1 event is irreversible.

For the experiments, the system contained approximately 800 bubbles in a planar shear cell with $L_y=9$ cm. The bubble raft was bidisperse consisting of a 4-to-1 ratio of 2.5 ± 0.3 to 5.3 ± 0.5 mm diameter bubbles. We report on results using driving amplitudes A of 10 and 12 times the diameter of the small bubbles and driving frequency 0.2 s^{-1}. The resulting rms strain and strain rate were approximately 0.2 and 0.04 s^{-1}, respectively. For comparison, the yield

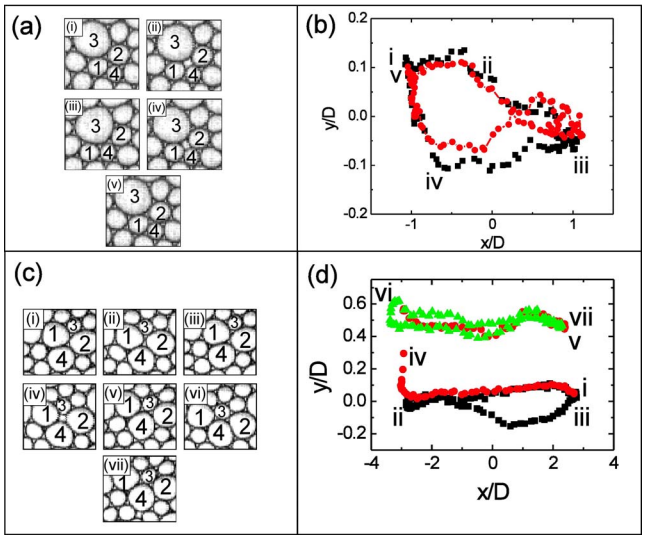

FIG. 1. (Color online) Experimental results for a reversible [(a) and (b)] and an irreversible T1 event [(c) and (d)]. The images in (a) and (c) are 10.5×10.5 mm^2 with bubbles involved in the T1 events labeled by numbers. The roman label for each image in (a) and (c) corresponds to the same label on the trajectory in (b) and (d). (a) The images highlight the following stages of the reversible T1 event: initial state (i), middle of the T1 event (ii), second state (iii), middle of the T1 event under reversal of shear (iv), and the return to the initial state (v) [37]. (b) Plot of the trajectory of bubble 1 in the images in (a). Two consecutive cycles are shown (the first in black squares and the second in red circles). (c) The images highlight the following stages of the irreversible T1 event: initial state (i)–(iii), middle of the T1 event (iv), and the second state (v)–(vii). (d) Plot of the trajectory of bubble 4 in the images in (c). Three consecutive cycles are shown (the first in black squares, the second in red circles, the third in green triangles).

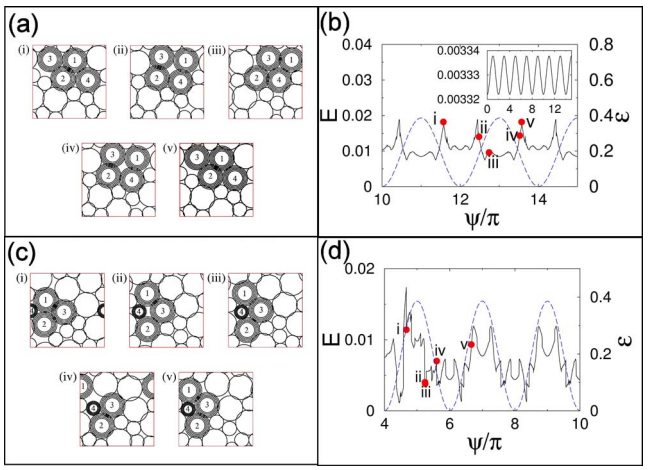

FIG. 2. (Color online) Results taken from a 16-particle simulation of the bubble model in two dimensions undergoing oscillatory shear strain with an amplitude of two small bubble diameters for a reversible [(a) and (b)] and an irreversible event [(c) and (d)]. Bubbles involved in the T1 events are labeled by numbers. Roman labels in the images correspond to the same labels in the plots. (a) Images (i)–(iii) show the occurrence of a reversible T1 event and (iv) and (v) show the reversal of the T1 event. (See the supplementary information [37] for a movie of this event.) (b) The local potential energy E (solid black line) is plotted versus the driving phase (left axis). For comparison, the periodic strain is plotted with a long dashed blue line (right axis). The elapsed phase for the T1 event is significantly different than that for the reversed T1 event, and the shape of the local potential energy is not the same for the T1 event and its reverse. The inset shows an elastic response in E vs ψ/π for small amplitude oscillations $A=10^{-2}$ times the small bubble diameter, where the response matches the driving. (c) Images (i)–(iii) show the occurrence of an irreversible T1 event, as shown by the absence of the reverse T1 event in images (iv) and (v) [37]. (d) The local potential energy E (solid black line) is plotted versus the driving phase (left axis). The periodic strain is plotted with a long dashed blue line (right axis). Note that E for locations (i) and (v) separated by a phase interval of 2π are not the same.

strain is 0.01 for bubble rafts and the transition to quasistatic behavior is on the order of 0.07 s^{-1} [32]. Beyond the yield strain, a cascade of T1 events gives rise to permanent plastic deformation [28,31,33,34]. Details of the experimental setup for the bubble rafts can be found in Ref. [35].

The bubble model simulations used bidisperse systems composed of $N/2$ large and $N/2$ small circular bubbles with diameter ratio $r=1.75$, which matches the experiments. We studied square simulation cells with system sizes in the range $N=16$–1024 and packing fraction $\phi=0.95$. The bubbles are treated as massless deformable disks with an equation of motion that balances a linear repulsive spring force to model elastic repulsion with viscous dissipation proportional to local velocity differences [22]. Oscillatory shear strain with amplitudes up to eight times the small bubble diameter is applied quasistatically to the system by shifting the x positions of the bubbles, implementing shear-periodic Lees-Edwards boundary conditions [36] and minimizing the total potential energy. To study the role of the potential energy landscape, two definitions of the local potential energy based on the overlaps between bubbles were used, E and E'. E is computed only considering overlaps among the four bubbles defining the T1 event, while E' also includes overlaps with the first nearest neighbors of the T1 bubbles. Finally, we measured $\Delta E'$, defined by subtracting the potential energy E' of the four bubbles participating in the reversible T1 event with E' from simulations in which the four T1 bubbles are forced to exactly retrace their positions as they transition from state B back to state A, but all other particles are allowed to move without constraints.

We directly compare the reversible and irreversible rearrangement events from experiments and simulation. Figures 1(a) and 1(b) (experiment) and Figs. 2(a) and 2(b) (simulation) highlight typical reversible T1 events. Figures 1(c) and 1(d) (experiment) and Figs. 2(c) and 2(d) (simulation) highlight irreversible events. The plots focus on the four bubbles (labeled 1–4) in the T1 event. Snapshots illustrate bubble motions during a typical T1 event [panels (a) and (c)]. For the experiments, panels (b) and (d) highlight the trajectory of a single bubble in real space. For the simulations, panels (b) and (d) display the potential energy E as a function of the phase of the driving. The simulation results are for $N=16$, but similar results were obtained with much larger systems with $N=1024$.

For reversible T1 events, the initial and final states of the bubbles in the T1 event are equivalent, despite the occurrence of dissipation. The dissipation is evident in the out-of-phase/asynchronous response of the potential energy behavior with respect to the drive. [For contrast, perfectly elastic behavior that is observed for small shear strains with no T1 events is shown in the inset of Fig. 2(b).] Dissipation leads to a number of asymmetries in the dynamics, despite the overall periodic nature of the response. The spatial trajectory is a closed loop with a finite area [see Fig. 1(b)]; and similar arrangements of the four bubbles during the two T1 events [images (ii) and (iv) in Fig. 1(a)] occur at different phases during the corresponding half-cycle. Likewise, Fig. 2(b) illustrates that E is very different for the two half-cycles corresponding to labels (i)–(iii) and (iv) and (v). Finally, the durations of the T1 event and its reverse (state A to B vs state B to A) are not the same.

During irreversible T1 events, a foursome of bubbles undergoes a T1 event in the first half-cycle of the driving but the reverse T1 event does not occur during the second half-cycle. The experimental example in Fig. 1(c) is a case where a T1 event from state A to B occurred during one out of seven cycles of the driving [three of which are highlighted in Fig. 1(c)]. The impact of the T1 event on the trajectories is dramatic [Fig. 1(d)]. The trajectory of bubble four is shown for three cycles: just before the T1 event (black squares), during the T1 event (red circles), and just after the T1 event (green triangles). In the absence of a T1 event, the local trajectory essentially repeats itself during each half-cycle as the bubbles move along similar paths. The occurrence of the T1 event represents a dramatic break in this motion. Similar motions are observed in the simulations. Figure 2(c) illustrates a T1 event in the simulation that occurs during the first half-cycle of driving (images i–iii), but not during the second half-cycle (images iii–v). The plot of E in Fig. 2(d) illustrates that configurations (i) and (v), which are separated by 2π in phase, do not have the same local potential energy.

An important next step is the characterization of the fraction of irreversible vs reversible T1 events. During an initial transient regime, irreversible events dominate over reversible events, and the fraction of irreversible events is highly cycle dependent. (In both simulation and experiment, the transient regime is two cycles, and ten additional cycles of steady state behavior is studied.) In the simulations, the fraction of irreversible events in steady state increases with increasing strain amplitude. For low amplitudes, but beyond the yield strain, the fraction is approximately 10%, and it reaches 60% at six times the small bubble diameter. Similar results are found in experiments, but the measurements have limited statistics. Thus reversible and irreversible T1 events coexist at small amplitudes, but irreversible events dominate at large amplitudes.

Using simulations, we also investigated the connection between reversible T1 events and the system's path through the potential energy landscape. By calculating $\Delta E'$ obtained by comparing the local potential energy E' (including interactions of T1 bubbles with first nearest neighbors) of the four bubbles in the original oscillatory shear strain simulations with E' from the constrained simulations, we were able to analyze the motion of the system through the potential energy landscape. The local potential energy difference averaged over many reversible T1 events from independent runs shows $\langle \Delta E' \rangle > 0$ [see Fig. 3(a)]. $\Delta E'$ for a single T1 event has large positive spikes with significant phase intervals where $\Delta E' = 0$ [inset in Fig. 3(a)]. The distribution of energy differences, $P(\Delta E')$, has a strong peak at zero, but non-negligible peaks at $\Delta E' \approx 0.15$ and 0.3 and no significant weight for $\Delta E' < 0$ [Fig. 3(b)]. These findings show that there are instances during the second half-cycle for which it is energetically favorable for the system to deviate from the path followed in configuration space during the first half-cycle.

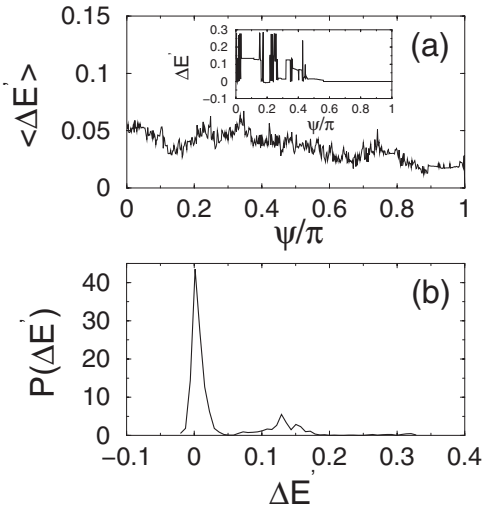

FIG. 3. (a) The local potential energy difference $\langle \Delta E' \rangle$ averaged over 100 reversible T1 events plotted vs the driving phase under the same conditions in Fig. 2. $\langle \Delta E' \rangle > 0$ confirms that *exact* trajectory reversal is not energetically favorable. The inset shows $\Delta E'$ for a single reversible T1 event. (b) The probability of finding a particular $\Delta E'$. There is a large peak at $\Delta E' = 0$, two slight peaks near 0.15 and 0.30, and no significant weight in the distribution for $\Delta E' < 0$.

From this analysis, we learn that the system can move from one potential energy minimum to another along many different routes and that the system chooses a particular route by minimizing the local potential energy arising from bubble overlap. For example, during the first half-cycle of the applied strain, the system can follow a particular path *into* a minimum, but upon strain reversal, the system may find a different path with lower energy that allows the system to move away from the original minimum. For reversible T1 events, there is a low energy pathway that leads from state B back to state A. For irreversible T1 events, the low energy pathways away from state B do not return to state A. Since our system is athermal, T1 events will likely be irreversible if the bubbles surrounding those in the T1 event undergo significant rearrangements during the first half-cycle.

In this work, we have visualized reversible T1 rearrangement events in 2D foam as well as studied the transition from an elastic deformation with mostly reversible T1 events to macroscopic plastic flow with mainly irreversible T1 events. This is a direct experimental confirmation of reversible microscopic plastic zones or shear transformation zones (STZs). The concept of a STZ as a reversible, two-state tran-

sition within a material that can be created or destroyed was first proposed by Falk and Langer [12]. The STZ picture is successful in explaining a range of macroscopic behavior of materials based on dynamics of STZs. The STZ framework represents a natural extension of ideas based on activated transitions and free volume [1,38,39] and has motivated a number of other models of plasticity [16,33,40]. Thus our results demonstrate the importance of including reversible microscopic plastic events (e.g., STZs) in models of plasticity in athermal particulate systems. In addition, our studies of the local potential energy landscape go beyond two-state models for plasticity and highlight the importance of the potential energy landscape in understanding the transition from reversible to irreversible microscopic plastic events.

Financial support from the Department of Energy [Grant Nos. DE-FG02-03ED46071 (M.D.), DE-FG02-05ER46199 (N.X.), and DE-FG02-03ER46088 (N.X.)], NSF [Grant Nos. DMR-0448838 (C.S.O.) and CBET-0625149 (C.S.O.)], and the Institute for Complex Adaptive Matter (K.K.) is gratefully acknowledged. We thank M. Falk for insightful conversations.

[1] A. S. Argon, Acta Metall. **27**, 47 (1979).
[2] M. L. Falk, J. S. Langer, and L. Pechenik, Phys. Rev. E **70**, 011507 (2004).
[3] M. D. Ediger, Annu. Rev. Phys. Chem. **51**, 99 (2000).
[4] D. Weaire and S. Hutzler, *The Physics of Foams* (Clarendon Press, Oxford, 1999).
[5] C. H. Liu and S. R. Nagel, Phys. Rev. B **48**, 15646 (1993).
[6] E. R. Weeks, J. C. Crocker, A. C. Levitt, A. Schofield, and D. A. Weitz, Science **287**, 627 (2000).
[7] E. R. Weeks and D. A. Weitz, Phys. Rev. Lett. **89**, 095704 (2002).
[8] T. G. Mason, J. Bibette, and D. A. Weitz, J. Colloid Interface Sci. **179**, 439 (1996).
[9] J. R. Rice and R. Thomson, Philos. Mag. **29**, 73 (1974).
[10] J. R. Rice, J. Mech. Phys. Solids **40**, 239 (1992).
[11] J. C. Baret, D. Vandembroucq, and S. Roux, Phys. Rev. Lett. **89**, 195506 (2002).
[12] M. L. Falk and J. S. Langer, Phys. Rev. E **57**, 7192 (1998).
[13] M. Heggen, F. Spaepen, and M. Feuerbacher, J. Appl. Phys. **97**, 033506 (2005).
[14] J. S. Langer, Phys. Rev. E **73**, 041504 (2006).
[15] A. Onuki, Phys. Rev. E **68**, 061502 (2003).
[16] G. Picard, A. Ajdari, L. Bocquet, and F. Lequeux, Phys. Rev. E **66**, 051501 (2002).
[17] Cyclic experiments have been used to study the *macroscopic* response of foam [34]. These experiments show hysteric stress-strain curves similar to that observed in other plastic materials. Though related, these measurements do not provide insight into the microscopic events focused on here.
[18] L. Bragg, J. Sci. Instrum. **19**, 148 (1942).
[19] A. S. Argon and H. Y. Kuo, Mater. Sci. Eng. **39**, 101 (1979).
[20] A. Abdel Kader and J. C. Earnshaw, Phys. Rev. Lett. **82**, 2610 (1999).
[21] M. Dennin, Phys. Rev. E **70**, 041406 (2004).
[22] D. J. Durian, Phys. Rev. Lett. **75**, 4780 (1995).
[23] J. Lauridsen, M. Twardos, and M. Dennin, Phys. Rev. Lett. **89**, 098303 (2002).
[24] A. D. Gopal and D. J. Durian, Phys. Rev. Lett. **75**, 2610 (1995).
[25] Y. Wang, K. Krishan, and M. Dennin, Philos. Mag. Lett. **87**, 125 (2007).
[26] M. Dennin and C. M. Knobler, Phys. Rev. Lett. **78**, 2485 (1997).
[27] B. Dollet, M. Durth, and F. Graner, Phys. Rev. E **73**, 061404 (2006).
[28] D. A. Reinelt and A. M. Kraynik, J. Rheol. **44**, 453 (2000).
[29] M. F. Vaz and S. J. Cox, Philos. Mag. Lett. **85**, 415 (2005).
[30] D. Weaire, F. Bolton, T. Herdtle, and H. Aref, Philos. Mag. Lett. **66**, 293 (1992).
[31] S. Vincent-Bonnieu, R. H. Hohler, and S. Cohen-Addad, Europhys. Lett. **74**, 533 (2006).
[32] E. Pratt and M. Dennin, Phys. Rev. E **67**, 051402 (2003).
[33] G. Picard, A. Ajdari, F. Lequeux, and L. Bocquet, Eur. Phys. J. E **15**, 371 (2004).
[34] S. Hutzler, Ph.D. thesis, Trinity College, Dublin, 1997 (unpublished).
[35] M. Lundberg, K. Krishan, N. Xu, C. S. O'Hern, and M. Dennin (unpublished).
[36] M. P. Allen and D. J. Tildesley, *Computer Simulation of Liquids* (Oxford University Press, Oxford, 1987).
[37] See EPAPS Document No. E-PLEEE8-77-132804 for movies of the reversible and irreversible events from both the experiments and simulation. For more information on EPAPS, see http://www.aip.org/pubservs/epaps.html.
[38] V. A. Khonik and A. T. Kosilov, J. Non-Cryst. Solids **170**, 270 (1994).
[39] F. Spaepen, Acta Metall. **25**, 407 (1977).
[40] L. Berthier, J. Phys.: Condens. Matter **15**, S933 (2003).